B@LGTs of Nd, Eu, Er, and Yb lanthanides with physicochemical interfacing for enhanced photocatalytic reduction of fluorescent dye, transition metal ions, and quinonoid phenolphthalein

*Krishan Kumar and Man Singh**

Krishan8053649040@gmail.com, Mansingh50@hotmail.com*

School of Chemical Sciences, Central University of Gujarat, Gandhinagar Sector-30 (382030), India

a. Characterization

UV/Vis, spectra recorded with Shimadzu UV1800 double beam spectrophotometer, X-ray diffraction (XRD) with Bruker Advance-D8 diffractometer with Cu Kα radiation ($\lambda = 0.15406\ \text{nm}, 40\ \text{kV}, 40\ \text{mA}$) source, BET spectra with Surfer system-standard, (thermos scientific) have elucidated their electronic transition, lattice planes, and surface area respectively. Thermal stability and DSC were determined with TGA on (EXSTAR TG/DTA 7300) analyzer and DSC 6000, Perkin Elmer respectively in N_2 environment. FGs were analyzed with FT-IR spectrometer (Perkin Elmer, Spectrum 65), X-ray photoelectron spectroscopy (XPS) at RT at $\sim 10^{-9}$mbar with hemispherical electron energy analyser (Phoibos 100 from Specs GmbH). HR-TEM and SEM images were analysed with JEOL JEM 2100 TEM HR LaB6 Version, JEOL, and EVO 18, (Carl Zeiss) respectively; and Raman spectroscopy (VGS, 50-4000 cm^{-1}, 4K with Liquid He). PCPs and density with Borosil Mansingh Survismeter (Cal.06070582/1.01/C–0395,NPL,GOI) and Anton par Densimeter-5000, respectively.

b. BBR Dye, metal salt, and QHIn solution preparations

Aq-BBR dye (1g/L) stock solution was used for dilutions. The 20 mg/100mL of $CrCl_3$, $NiCl_2$, and $CuCl_2$ were separately prepared. The 2 mg HIn and 1mg NaOH in 100 mL water resulting QHIn at $pH = 9$ used for PCR with 0.010g/100 mL B@LGTs photocatalyst.

c. PCR experiments for BBR, TMIs, and QHIn

PCR of BBR, TMIs, and QHIn were conducted under sunlight with 680 W/m² (Solar meter, KM-SPM-11) from 12.00 am to 1.00 pm Gandhinagar, Gujarat, India. The 0.008-0.012 @0.01g% $B@Nd_2S_3:GO$, $B@Eu_2S_3:GO$, $B@Er_2S_3:GO$, and $B@Yb_2S_3:GO$ separately were mixed with each of BBR, TMIs, and QHIn 10-80 ppm @10 ppm in 2-12 pH. It has found the pH 7, 0.010g% B@LGTs, and 40 ppm BBR, 20 ppm TMIs, and QHIn for maximum PCR. The 10 mL B@LGTs mixed separately with 100mL each of BBR, TMIs, and QHIn were kept in sunlight for 1h. The 5 mL aliquot after 5 min was centrifuged, and its UV/Vis absorption was recorded for determining their residual conc. After every 5 min, an aliquot was collected for recording UV/Vis, it continued till a complete reduction occurred that gave a zero absorption to calculate PCR rate constant[1].

PCR @ (%) = $\frac{C_0 - C_t}{C_0} \times 100$, C_t/C_0 vs t, and $\ln(C_0/C_t) = kt$ (1.0)

C_0, initial conc. at t = 0 and C_t reduced at t min, k is rate constant calculated from slope of $\ln(C_0/C_t)$ vs time 't' fit in **eqn. (1.0).**

Fig. S1. (a) $KMnO_4$ and Gt (b) with H_2SO_4 (c) refluxed for 12h (d) washed with cold water (e) with H_2O_2 (f) exfoliated GO sheet (g) GO powder.

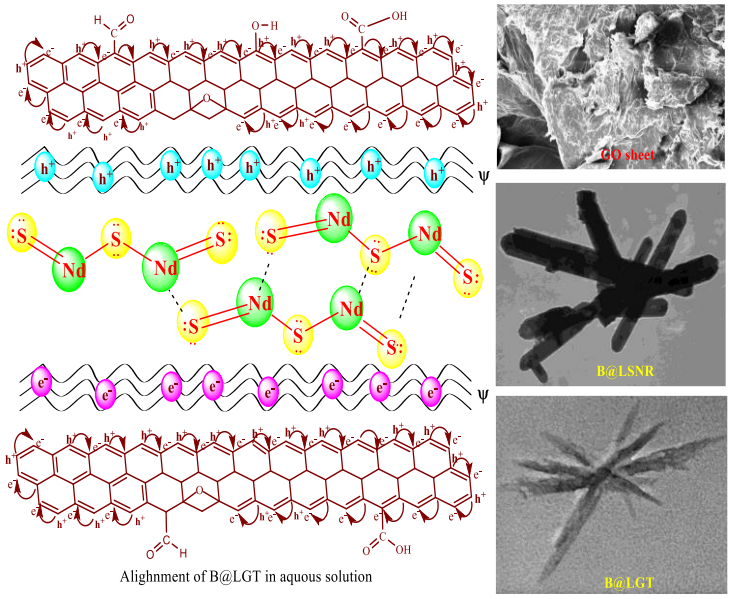

Fig. S2. The B@LGTs in aq-solution with probable LSNR and 2D GO sheet alignment for generating the e^- and h^+ holes to PCR the dye, TMIs, and QHIn.

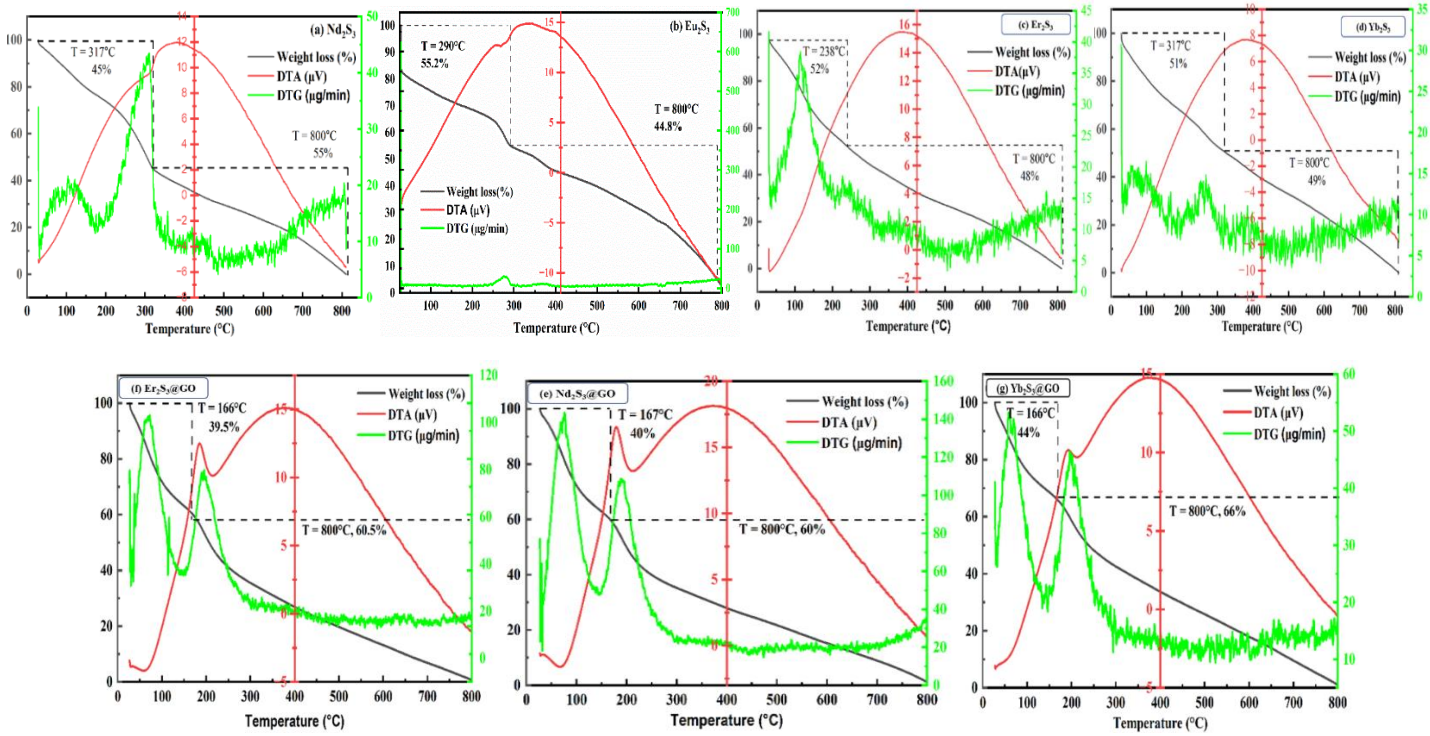

Fig. S3. The TGA, DTA and DTG analysis from (a) to (d) for LSNR while from (f) to (g) with two prominent wt loss DTG peaks for LGT distinguishing a coating.

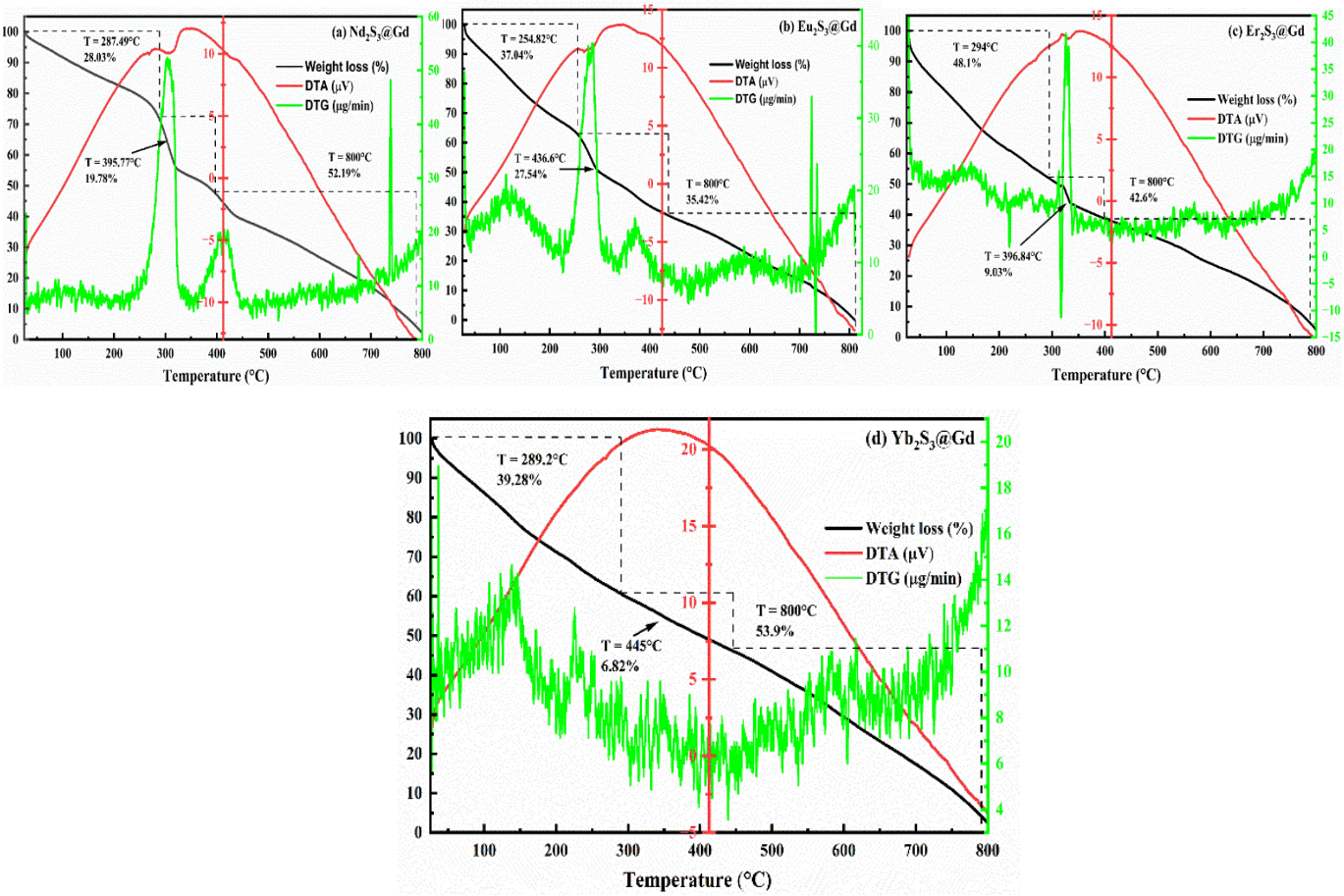

Fig. S4. Varying DTG patterns from (a) to (d) differentiating the spinning of increasing 4f electrons for B@LSNR under TGA analysis

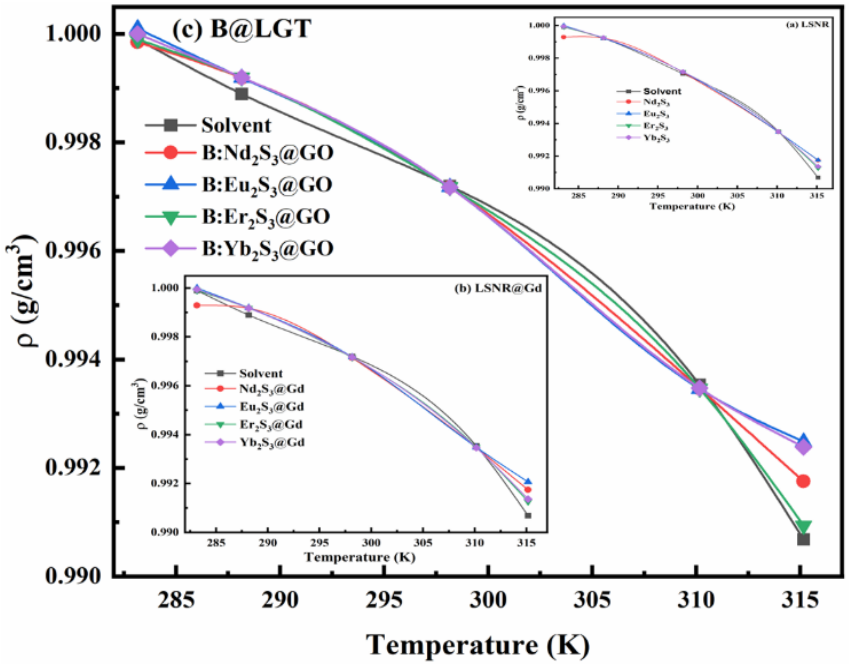

Fig. S5. The density values for (a) LSNR (b) B@LSNR (c) B@LGT at increasing temperature with negative slope values and comparatively more scattering at 315K.

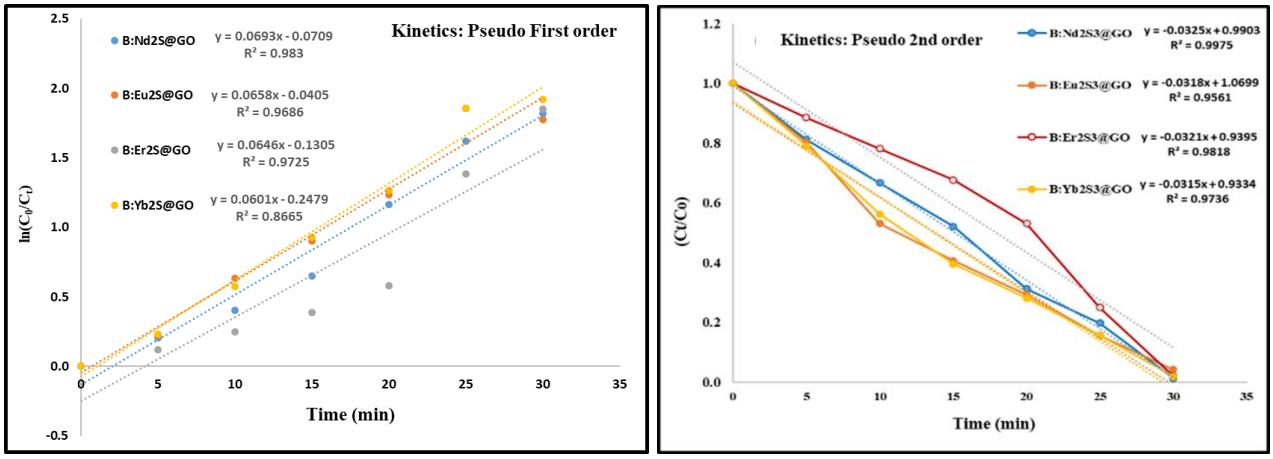

Figs. S6. The plots of $ln(c_0/c_t)$ vs time and (c_0/c_t) vs time at pH =7 with 1st order kinetics due to physisorption without structural damage photocatalysts during PCR.

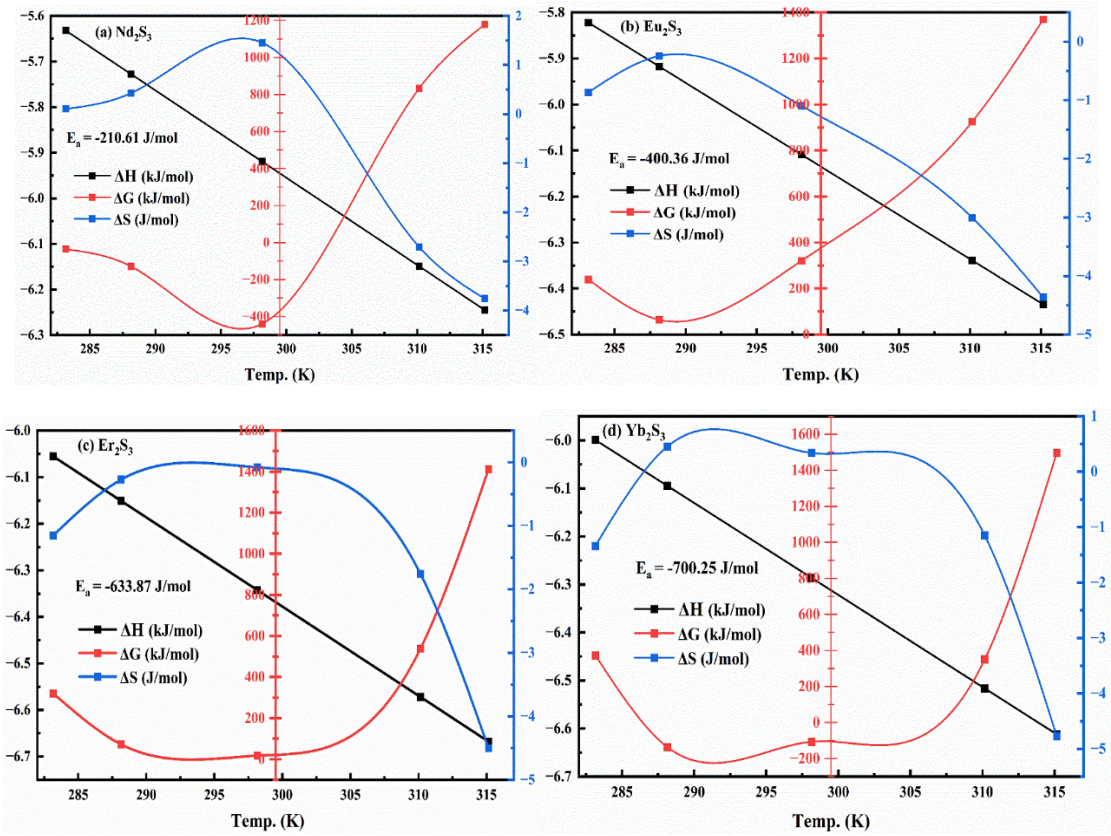

Fig. S7. For LSNR, the dH from (a) to (d) linearly decreased while the dG and dS oppositely vary on release of heat content on increasing temperature with reorientations.

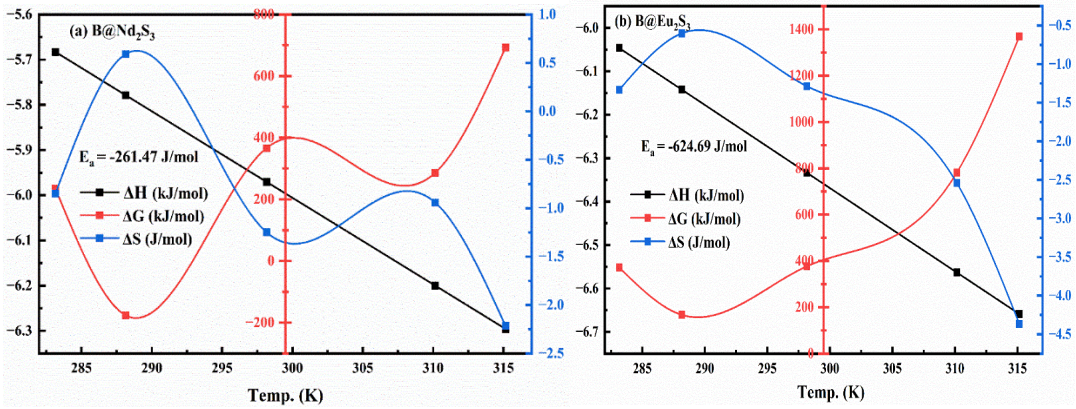

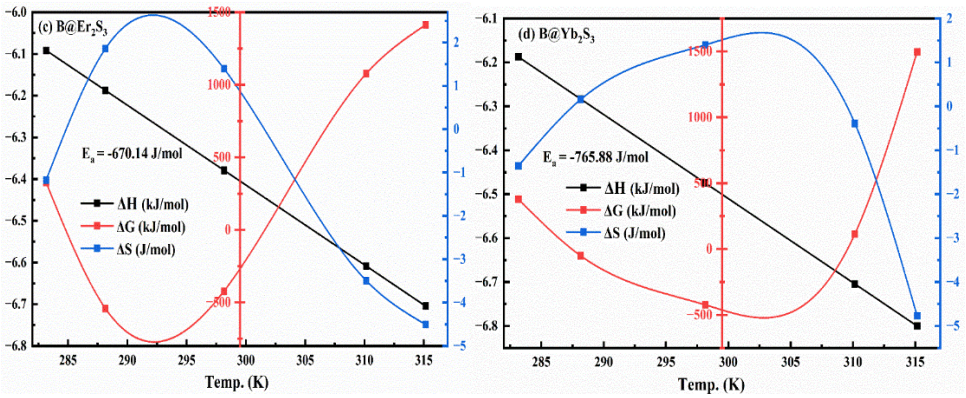

Fig. S8. For B@LSNR, the dH from (a) to (d) linearly decreased while the dG and dS oppositely vary due to mutual conversion with two common intersections credited to dopant.

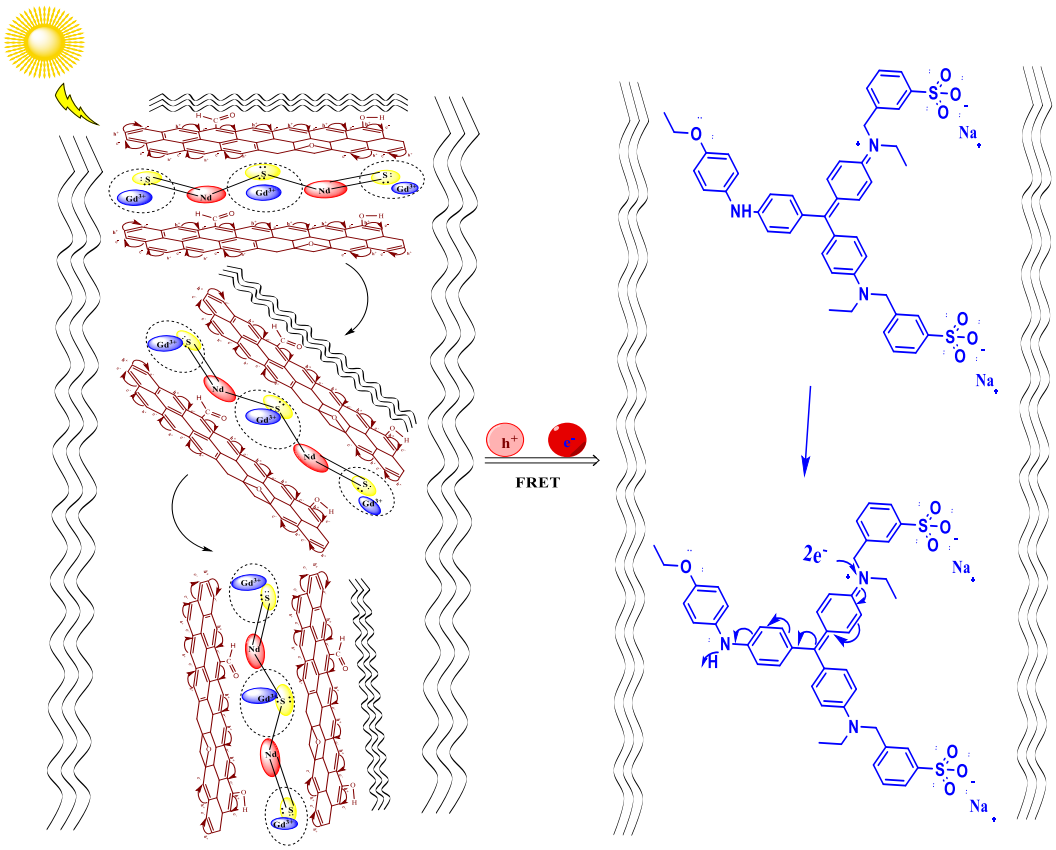

Fig. S9. The rotational, vibrational, and translational motions for electrostatically stabilization of monodispersed B@LGT tentropically aligned to receive hv for PCR mechanism.

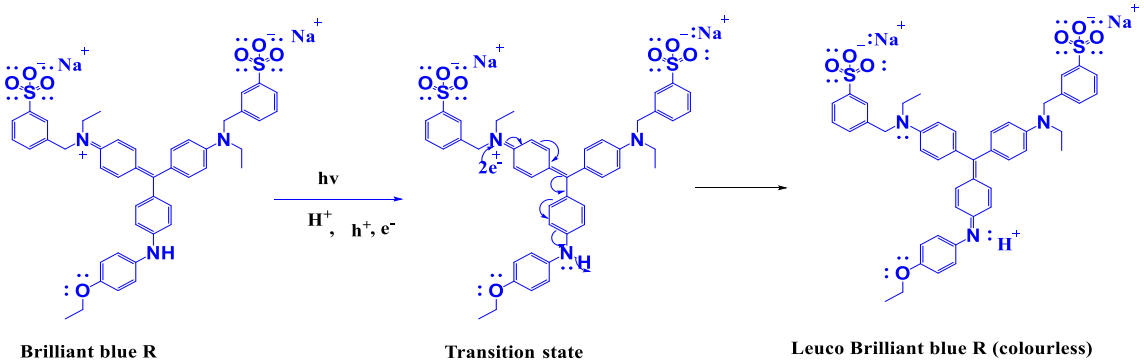

Fig. S10. Respective electrostatic sites of dye shifting from one to other energy state for attaining optimum energy for receiving receive holes and hv.

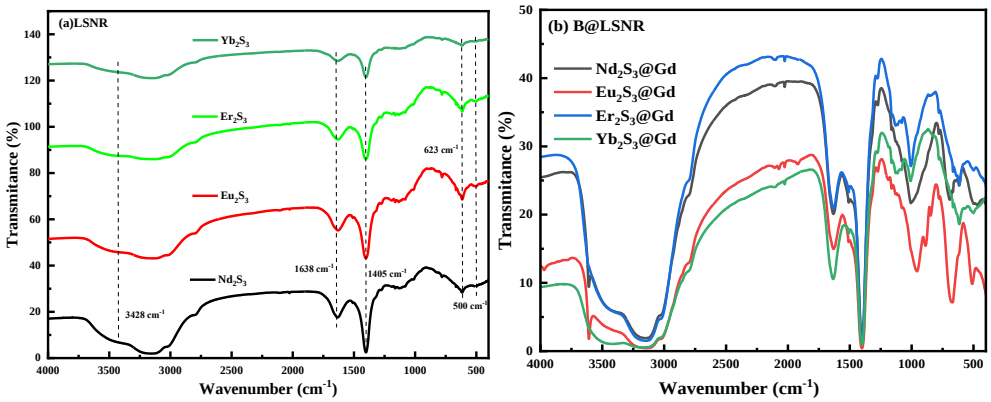

Fig. S11. FT-IR spectra Illustrating stretching and bending frequencies with LSNR and B@LSNR for comparative study on increasing their 4f electrons..

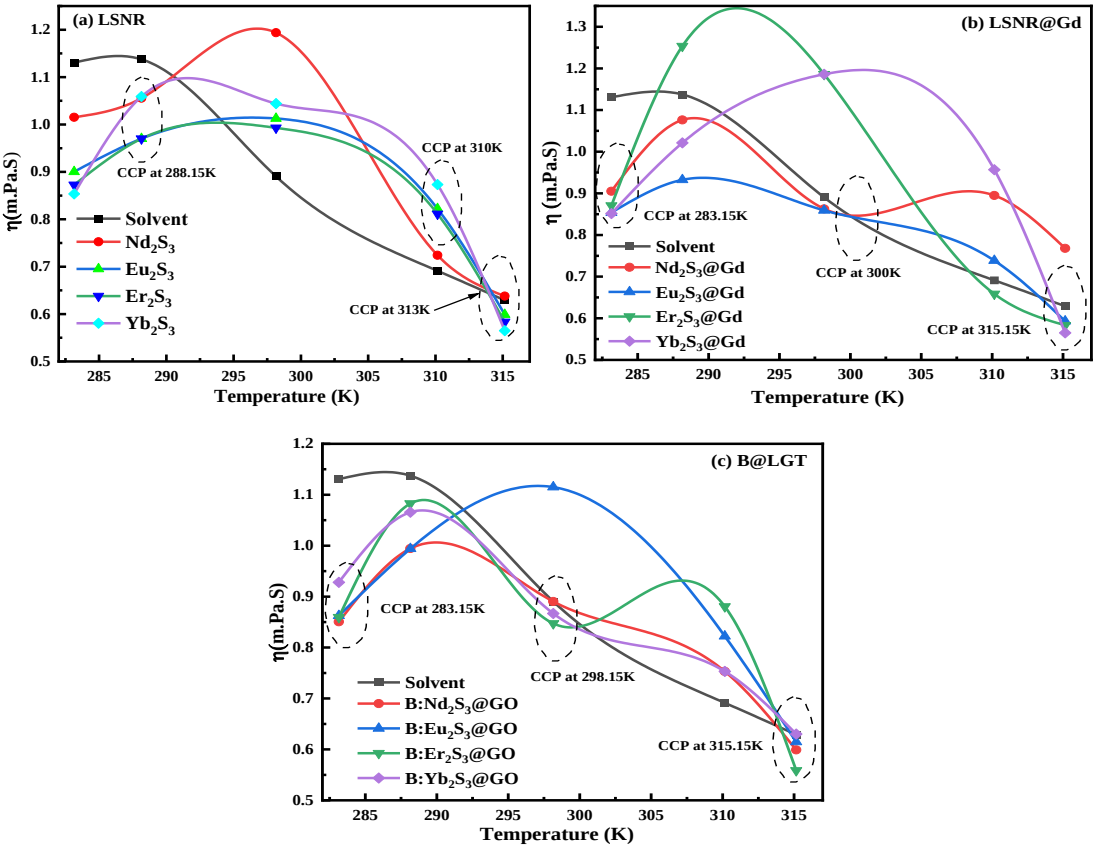

Fig. S12. The viscosities for (a) aq-LSNR (b) aq-B@LSNR (c) aq-B@LGT plotted against temperatures with higher resolution for B@LSNRs while the values of B@LGTs in narrow range.

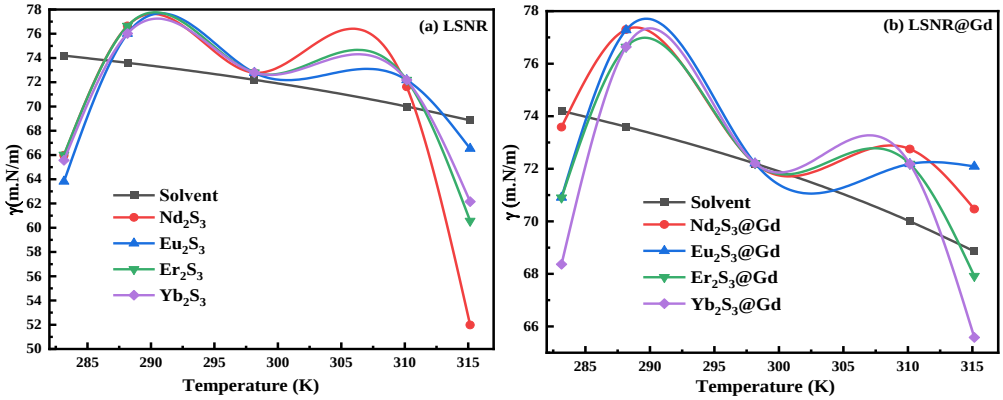

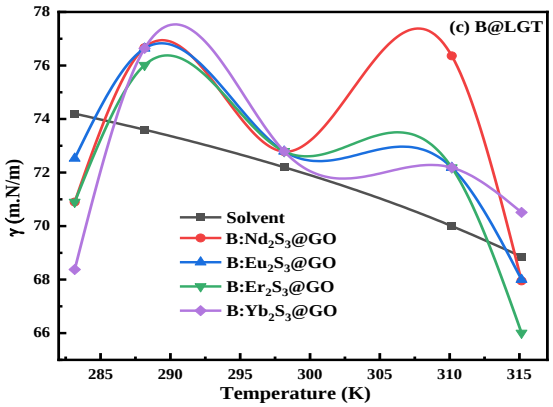

Fig. S13. The surface tension (a) aq-LSNR (b) aq-B@LSNR (c) aq-B@LGT plotted against temperatures with higher resolution for B@LSNRs while the values of B@LGTs in narrow range.

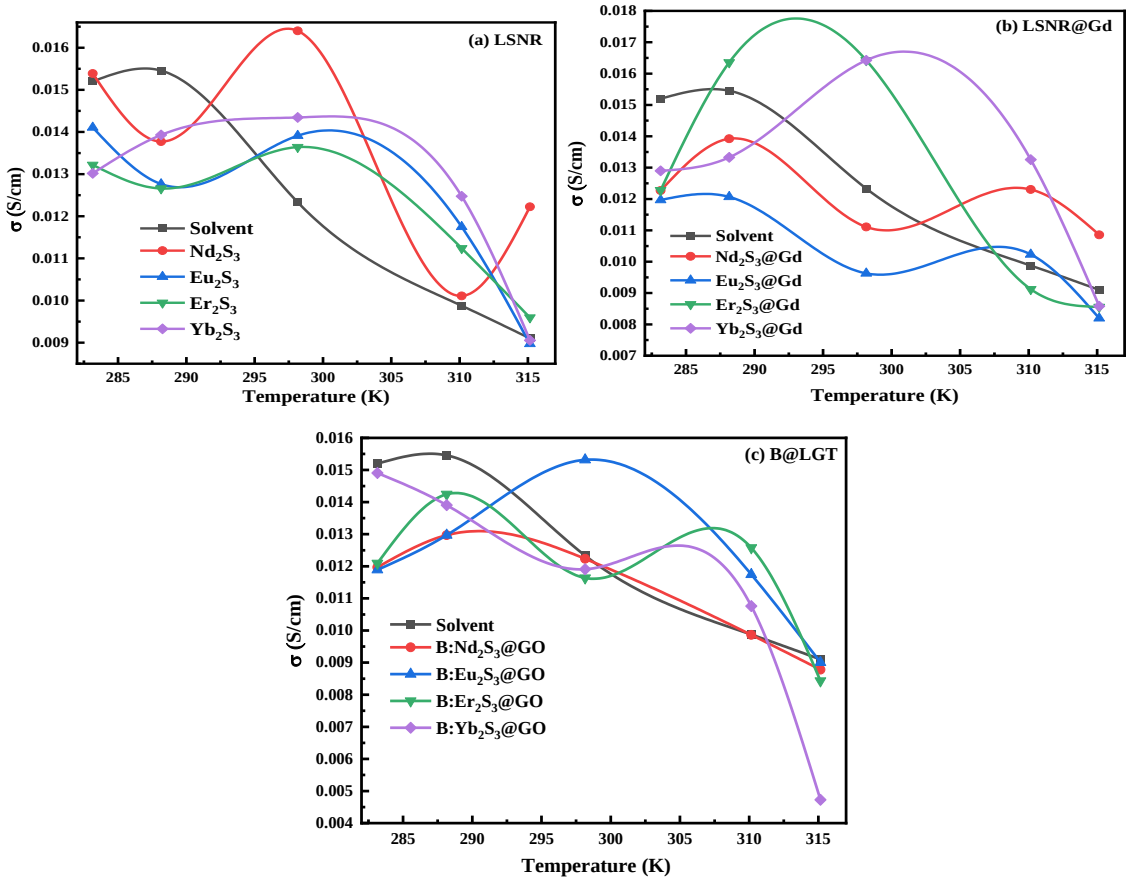

Fig. S14. Friccohesity (a) aq-LSNR (b) aq-B@LSNR (c) aq-B@LGT plotted against temperatures with higher resolution for LSNR and B@LSNRs while the values of B@LGTs in narrow range.

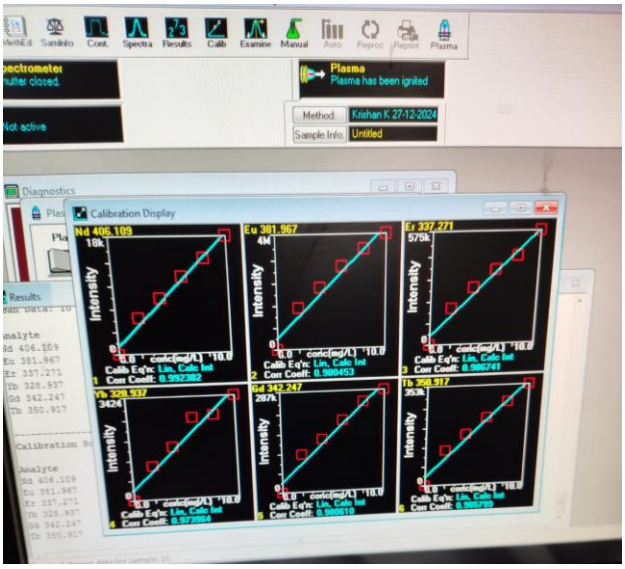

Fig. S15. Regression constants (R^2) with the standard solutions of the $NdCl_3$, $EuCl_3$, $ErCl_3$, $YbCl_3$, and $GdCl_3$ salts by using 2-10 ppm @2 ppm for calibration to analyse ICP-OES for the elemental composition of the LSNR, B@LSNRs, and B@LGTs.

Tables:

Table S1. The PDN values for aq-LSNR and aq-B@LSNR solutions at variable temperatures.

Temp.(K)	Nd_2S_3	Eu_2S_3	Er_2S_3	Yb_2S_3	$Nd_2S_3@Gd$	$Eu_2S_3@Gd$	$Er_2S_3@Gd$	$Yb_2S_3@Gd$
283.15	145	150	145	146	130	135	135	140
288.15	121	122	121	122	120	120	121	121
298.15	124	124	124	124	125	125	125	125
310.15	129	128	128	128	127	128	128	128
315.15	153	143	157	153	135	132	140	145

Table S2. The PDN values for aq-B@LGT solutions at variable temperatures.

Temp.(K)	$B: Nd_2S_3@GO$	$B: Eu_2S_3@GO$	$B: Er_2S_3@GO$	$B: Yb_2S_3@GO$
283.15	135	132	135	140
288.15	121	121	122	121
298.15	124	124	124	124
310.15	121	128	128	128
315.15	140	140	144	135

Table S3. The viscous flow time values for aq-LSNR and aq-B@LSNR solutions at variable temperatures.

Temp.(K)	Nd_2S_3	Eu_2S_3	Er_2S_3	Yb_2S_3	$Nd_2S_3@Gd$	$Eu_2S_3@Gd$	$Er_2S_3@Gd$	$Yb_2S_3@Gd$
283.15	370	328	318	311	330	310	318	311
288.15	309	284	284	310	315	273	367	299
298.15	303	257	252	265	219	218	301	301
310.15	199	226	223	240	246	203	181	263
315.15	208	195	190	184	250	193	190	184

able S4. The viscous flow time values for aq-B@LGT solutions at variable temperatures.

Temp.(K)	$B: Nd_2S_3@GO$	$B: Eu_2S_3@GO$	$B: Er_2S_3@GO$	$B: Yb_2S_3@GO$
283.15	310	315	314	339
288.15	291	291	317	312
298.15	226	283	215	220
310.15	207	226	242	207
315.15	195	200	182	205

Table S5. The density values for aq-LSNR and aq-B@LSNR solutions at variable temperatures.

Temp.(K)	Nd_2S_3	Eu_2S_3	Er_2S_3	Yb_2S_3	$Nd_2S_3@Gd$	$Eu_2S_3@Gd$	$Er_2S_3@Gd$	$Yb_2S_3@Gd$
283.15	0.999292	1	0.999900	0.999940	0.999292	1	0.999900	0.999940
288.15	0.999228	0.999218	0.99925	0.999251	0.999170	0.999192	0.999171	0.999174
298.15	0.99712	0.997151	0.997168	0.997167	0.997139	0.997177	0.997153	0.997168
310.15	0.993473	0.993476	0.993501	0.993502	0.993465	0.993482	0.993483	0.993464
315.15	0.991740	0.991752	0.99126	0.99136	0.991740	0.992064	0.99126	0.991360

Table S6. The density values for aq-B@LGTs solutions at variable temperatures.

Temp.(K)	$B: Nd_2S_3@GO$	$B: Eu_2S_3@GO$	$B: Er_2S_3@GO$	$B: Yb_2S_3@GO$
283.15	0.999848	1.000100	0.999900	1.000000
288.15	0.999191	0.999194	0.999198	0.999200
298.15	0.997173	0.997176	0.997176	0.997176
310.15	0.993468	0.993458	0.993463	0.993469
315.15	0.991752	0.992484	0.990940	0.992384

Table S7. The ΔG, ΔH and ΔS for E_α =-3.95 J/mol values determined from UV/Vis abs for PCR of BBR with aq-$B: Nd_2S_3@GO$ under S at variable time.

Time (min)	C_t (ppm)	ΔH (kJ/mol)	ΔG (kJ/mol)	ΔS (J/mol)	Φ (%)
5	30.55	-99.6934	-10.3837385	-17.86193715	18.85
10	25.33	-195.429	-36.33504925	-15.9094085	32.71
15	22.94	-291.165	-66.87449544	-14.95268992	39.06
20	14.98	-386.901	-160.0458427	-11.34273558	60.21
25	7.80	-482.636	-335.6239927	-5.880490861	79.27
30	1.37	-578.372	-836.3080769	8.597870089	96.35

Table S8. The ΔG, ΔH and ΔS for E_a =-3.93 J/mol values determined from UV/Vis abs for PCR of BBR with $B: Eu_2S_3@GO$ under SL at variable time.

Time (min)	C_t (ppm)	ΔH (kJ/mol)	ΔG (kJ/mol)	ΔS (J/mol)	Φ (%)
5	30.20	-99.6724	-10.86689102	-17.76109428	19.79
10	16.35	-195.408	-72.73308896	-12.26749834	56.56
15	16.00	-291.144	-111.8211772	-11.95484035	57.50
20	14.75	-386.879	-162.6787731	-11.21003596	60.83
25	7.76	-482.615	-336.6712869	-5.83775662	79.38
30	1.25	-578.351	-858.663169	9.343741887	96.67

Table S9. The ΔG, ΔH and ΔS for E_a =-4.29 J/mol values determined from UV/Vis abs for PCR of BBR with of $B: Er_2S_3@GO$ under SL at variable time.

Time (min)	C_t (ppm)	ΔH (kJ/mol)	ΔG (kJ/mol)	ΔS (J/mol)	Φ (%)
5	31.57	-100.032	-9.018698278	-18.20272608	16.15
10	31.02	-195.768	-19.49629329	-17.62717454	17.60
15	25.65	-291.504	-52.96738561	-15.9024242	31.88
20	16.39	-387.239	-145.0678305	-12.10858141	56.46
25	9.49	-482.975	-294.9543671	-7.520832061	74.79
30	0.90	-578.711	-941.0468928	12.07786714	97.60

Table S10. The ΔG, ΔH and ΔS for E_a =-30.12 J/mol values determined from UV/Vis abs for PCR of BBR with $B: Yb_2S_3@GO$ under SL at variable time.

Time (min)	C_t (ppm)	ΔH (kJ/mol)	ΔG (kJ/mol)	ΔS (J/mol)	Φ (%)
5	26.82	-125.864	-15.79102121	-22.01454335	28.75
10	16.94	-221.599	-69.79444461	-15.18050033	55.00
15	9.57	-317.335	-175.9460098	-9.42594321	74.58
20	2.94	-413.071	-430.7872346	0.885818334	92.19
25	2.16	-508.807	-602.9613613	3.766191335	94.27
30	0.31	-604.542	-1204.495013	19.99842418	99.17

Table S11. The C, H, and S values for GO, B@LSNR, and B@LGT.

EuroEA Elemental Analyzer

AutoRun name : CIF-21DEC2022 (26)
Date of print : 21 Dec 2022
Time of print : 14:26:08

Balance Operator : EVR EVR CHNSLinear
Operator :
Configuration :

Calibration Type: *Results*
Summary for Element %

#	Type	Name	N %	C %	H %	S %	O %	Weight (mg)
1	Std	Sulphanilamide	16.308	41.846	4.663	18.659	-	1.440
2	Std	Sulphanilamide	16.165	41.720	4.688	18.691	-	1.177

3	Std	Sulphanilamide	16.271	41.963	4.717	18.500	-	1.275
4	Std	Sulphanilamide	16.294	41.794	4.657	18.649	-	0.990
5	Std	Sulphanilamide	16.306	41.926	4.690	18.608	-	0.766
6	Byp	Bypass	-	-	-	-	-	-
7	Byp	Bypass	-	-	-	-	-	-
8	Smp	Sulphanilamide SAMPLE-1	16.410	42.431	4.886	18.735	-	1.387
9	Smp	Sulphanilamide SAMPLE-2	16.331	42.650	5.027	18.479	-	0.788
10	Smp	Nd2S3@GD	-	-	-	1.105	-	1.116
11	Smp	Eu2S3@GD	-	-	-	1.116	-	1.097
12	Smp	Er2S3@GD	-	-	-	1.857	-	1.100
13	Smp	Yb2S3@GD	-	-	-	2.075	-	1.212
14	Smp	GO	-	60.558	3.306	-	-	1.0752
15	Smp	Nd2S3@Gd:GO	-	39.808	3.147	0.890	-	1.004
16	Smp	Eu2S3@Gd:GO	-	41.629	2.818	0.936	-	1.234
17	Smp	Er2S3@Gd:GO	-	40.978	3.098	0.797	-	1.365
18	Smp	Yb2S3@Gd:GO	-	41.698	2.381	1.045	-	1.380

Table S12. Variable d-spacing determined with theta values from XPS spectra of LSNR, B@LSNR, and B@LGT.

Systems	$2\theta_1(°)$, $d_1(nm)$	$2\theta_2(°)$, $d_2(nm)$	$2\theta_3(°)$, $d_3(nm)$	$2\theta_4(°)$, $d_4(nm)$	$2\theta_5(°)$, $d_5(nm)$	$2\theta_6(°)$, $d_6(nm)$	$2\theta_7(°)$, $d_7(nm)$	$2\theta_8(°)$, $d_8(nm)$	$2\theta_9(°)$, $d_9(nm)$
Nd_2S_3	10.47, 0.85	14.28, 0.61	15.94, 0.55	18, 0.49	23.5, 0.38	27.50, 0.32	28.78, 0.30	32, 0.28	40.4, 0.22
Eu_2S_3	9.44, 0.93	16.07, 0.55	28, 0.31	29.3, 0.30	32.5, 0.27	41, 0.22	43.44, 0.20	49.7, 0.18	50.5, 0.18
Er_2S_3	9.44, 0.93	20.5, 0.43	28, 0.30	33.88, 0.26	48.8, 0.18	57.8, 0.15	66.35, 0.14	68.2, 0.13	73, 0.12
Yb_2S_3	9.44, 0.93	19, 0.46	29, 0.30	48.4, 0.18	50.2, 0.18	51.7, 0.17	--	--	--
$Nd_2S_3@Gd$	10.42, 0.85	14.77, 0.59	15.89, 0.55	17.92, 0.49	23.34, 0.38	27.75, 0.32	28.73, 0.31	40.35, 0.22	49.67, 0.18
$Eu_2S_3@Gd$	9.38, 0.94	16.18, 0.54	28.11, 0.31	29.37, 0.30	32.5, 0.28	41.09, 0.22	49.71, 0.18	50.45, 0.18	58.24, 0.16
$Er_2S_3@Gd$	9.40, 0.94	16.38, 0.54	28.54, 0.31	30.11, 0.29	41.86, 0.21	51.45, 0.17	--	--	--
$Yb_2S_3@Gd$	9.48, 0.93	16.40, 0.54	25.54, 0.34	29.37, 0.30	30.28, 0.29	42.07, 0.21	51.55, 0.17	--	--

Table S13. The weight losses for Gt, GO, LSNR, B@LSNR, and B@LGT determined from TGA spectra in N_2 environment.

System	1^{st},wt (%) at Temp. ($°C$)	2^{nd},wt (%) at Temp. ($°C$)	3^{rd}·wt (%) at Temp. ($°C$)
Graphite	100%, T = 800 $°C$	-	-
GO	15.24%, T = 106$°C$	88.76%, T = 194$°C$	-
Nd_2S_3	45%, T = 317$°C$	55%, T = 800$°C$	-
Eu_2S_3	55.2%, T = 290$°C$	44.8%, T = 800$°C$	-
Er_2S_3	52%, T = 238$°C$	48%, T = 800$°C$	-
Yb_2S_3	51%, T = 317$°C$	49%, T = 800$°C$	-
$Nd_2S_3@Gd$	28.03%, T = 287.49$°C$	19.78%, T = 395.77$°C$	52.19%, T = 800$°C$
$Eu_2S_3@Gd$	37.04%, T = 254.82$°C$	27.54%, T = 436.6$°C$	35.42%, T = 800$°C$
$Er_2S_3@Gd$	48.1%, T = 294$°C$	9.03%, T = 396.84$°C$	42.6%, T = 800$°C$
$Yb_2S_3@Gd$	39.28%, T = 289.2$°C$	6.82%, T = 445$°C$	53.9%, T = 800$°C$
$B: Nd_2S_3@GO$	27.61%, T = 134.4$°C$	34.79%, T = 258.3$°C$	37.6%, T = 800$°C$
$B: Eu_2S_3@GO$	23.79%, T = 129$°C$	18.42%, T = 252.8$°C$	57.79%, T = 800$°C$
$B: Er_2S_3@GO$	28.7%, T = 143.8$°C$	23.79%, T = 265$°C$	47.51%, T = 800$°C$
$B: Yb_2S_3@GO$	24.05%, T = 142$°C$	38.76%, T = 246.9$°C$	37.19%, T = 800$°C$

Table S14. The ΔG, ΔH and ΔS for E_a = -210.61 J/mol values determined from viscosity values pf aq-Nd_2S_3 at variable temperatures

Temp.(K)	$\eta, (mPa.S)$	ΔH (kJ/mol)	ΔG (kJ/mol)	ΔS (J/mol)
283.15	1.0152	-5.63213	-35.484	0.10543
288.15	1.0555	-5.72787	-129.502	0.42955
298.15	1.1939	-5.91934	-439.300	1.45357
310.15	0.7240	-6.14910	832.876	-2.70522
315.15	0.6379	-6.24484	1178.233	-3.75846

Table S15. The ΔG, ΔH and ΔS for E_a = -400.36 J/mol values determined from viscosities of aq-Eu_2S_3 at variable temperatures.

Temp.(K)	$\eta, (mPa.S)$	ΔH (kJ/mol)	ΔG (kJ/mol)	ΔS (J/mol)
283.15	0.9035	-5.82188	238.9877	-0.86459
288.15	0.9736	-5.91762	64.04413	-0.2428
298.15	0.8787	-6.10909	320.5623	-1.09566
310.15	0.6986	-6.33885	925.1163	-3.00324
315.15	0.5930	-6.43459	1369.415	-4.3657

Table S16. The ΔG, ΔH and ΔS for E_a = -633.67 J/mol values determined from viscosities of aq-Er_2S_3 at variable temperatures

Temp.(K)	$\eta, (mPa.S)$	ΔH (kJ/mol)	ΔG (kJ/mol)	ΔS (J/mol)
283.15	0.8726	-6.055188	320.763594	-1.154225
288.15	0.9702	-6.150924	72.598207	-0.273292
298.15	0.9930	-6.342395	17.518568	-0.080030
310.15	0.8114	-6.572161	539.134678	-1.759493
315.15	0.5833	-6.667896	1412.594320	-4.503450

Table S17. The ΔG, ΔH and ΔS for E_a = -700.25 J/mol values determined from viscosities of aq-Yb_2S_3 at variable temperatures.

Temp.(K)	$\eta, (mPa.S)$	ΔH (kJ/mol)	ΔG (kJ/mol)	ΔS (J/mol)
283.15	0.8726	-6.055188	320.763594	-1.154225
288.15	0.9702	-6.150924	72.598207	-0.273292
298.15	0.9930	-6.342395	17.518568	-0.080030
310.15	0.8114	-6.572161	539.134678	-1.759493
315.15	0.5833	-6.667896	1412.594320	-4.503450

Table S18. The ΔG, ΔH and ΔS for E_a = -261.47 J/mol values determined from viscosities of aq-B@Nd_2S_3 at variable temperatures.

Temp.(K)	$\eta, (mPa.S)$	ΔH (kJ/mol)	ΔG (kJ/mol)	ΔS (J/mol)
283.15	0.9050	-5.68299	234.959996	-0.849878
288.15	1.0763	-5.77872	-176.208281	0.591461
298.15	0.8628	-5.97019	365.951801	-1.247432
310.15	0.8950	-6.19996	286.126131	-0.942531
315.15	0.7679	-6.29570	692.128414	-2.216164

Table S19. The ΔG, ΔH and ΔS for E_a = -624.69 J/mol values determined from viscosities of aq-B@Eu_2S_3 at variable temperatures.

Temp.(K)	$\eta, (mPa.S)$	ΔH (kJ/mol)	ΔG (kJ/mol)	ΔS (J/mol)
283.15	0.8539	-6.04621	371.8807	-1.33472
288.15	0.9325	-6.14194	167.3895	-0.60223
298.15	0.8590	-6.33342	376.8262	-1.28512
310.15	0.7386	-6.56318	781.5266	-2.541
315.15	0.5930	-6.65892	1369.415	-4.36641

Table S20. ΔG, ΔH and ΔS for E_a = -670.14 J/mol of values determined from viscosities of aq-B@Er_2S_3 at variable temperatures.

Temp.(K)	$\eta, (mPa.S)$	ΔH (kJ/mol)	ΔG (kJ/mol)	ΔS (J/mol)
283.15	0.8705	-6.091663	326.471557	-1.174513
288.15	1.2536	-6.187399	-541.545467	1.857915
298.15	1.1860	-6.378870	-422.962996	1.397230
310.15	0.6585	-6.608636	1077.364357	-3.494996
315.15	0.5833	-6.704372	1412.594320	-4.503566

Table S21. ΔG, ΔH and ΔS for E_a = -765.88 J/mol values determined from viscosities of $B@Yb_2S_3$ at variable temperatures.

Temp.(K)	$\eta, (mPa.S)$	ΔH (kJ/mol)	ΔG (kJ/mol)	ΔS (J/mol)
283.15	0.8514	-6.1874	378.785678	-1.35961
288.15	1.0213	-6.28313	-50.5457743	0.15361
298.15	1.1860	-6.47461	-423.000291	1.397034
310.15	0.9569	-6.70437	113.7329427	-0.38832
315.15	0.5650	-6.80011	1496.421535	-4.76986

Table S22. ΔG, ΔH and ΔS for E_a = -670.14 J/mol of values determined from viscosities of aq-B: Nd_2S_3@GO at variable temperatures.

Temp.(K)	$\eta, (mPa.S)$	ΔH (kJ/mol)	ΔG (kJ/mol)	ΔS (J/mol)
283.15	0.8506	-6.09166	380.856575	-1.366584
288.15	0.9943	-6.18739	13.6316331	-0.06878
298.15	0.8904	-6.37887	287.861459	-0.986887
310.15	0.7531	-6.60863	731.295537	-2.379185
315.15	0.5990	-6.70437	1343.22181	-4.28344

Table S23. ΔG, ΔH and ΔS for E_a = -767.39 J/mol values determined from viscosities of aq-B: Eu_2S_3@GO at variable temperatures.

Temp.(K)	$\eta, (mPa.S)$	ΔH (kJ/mol)	ΔG (kJ/mol)	ΔS (J/mol)
283.15	0.8625	-6.18891	348.3187	-1.25201
288.15	0.9940	-6.28465	14.38952	-0.07175
298.15	1.1151	-6.47612	-270.14	0.884334
310.15	0.8222	-6.70588	504.7818	-1.64916
315.15	0.6148	-6.80162	1274.94	-4.06708

Table S24. ΔG, ΔH and ΔS for E_a = -829.18 J/mol values determined from viscosities of aq-B: Er_2S_3@GO at variable temperatures.

Temp.(K)	$\eta, (mPa.S)$	ΔH (kJ/mol)	ΔG (kJ/mol)	ΔS (J/mol)
283.15	0.8596	-6.25070	356.276174	-1.28034
288.15	1.0828	-6.34644	-190.675652	0.639699
298.15	0.8472	-6.53791	411.183915	-1.40105
310.15	0.8805	-6.76767	328.354698	-1.08052
315.15	0.5586	-6.86341	1526.17307	-4.86447

Table S25. ΔG, ΔH and ΔS for E_a = -829.18 J/mol values determined from viscosities of B: Yb_2S_3@GO at variable temperatures.

Temp.(K)	$\eta, (mPa.S)$	ΔH (kJ/mol)	ΔG (kJ/mol)	ΔS (J/mol)
283.15	0.9281	-6.34709	175.6666907	-0.64282
288.15	1.0658	-6.44282	-152.585675	0.507176
298.15	0.8669	-6.63429	354.1867896	-1.2102
310.15	0.7531	-6.86406	731.2358323	-2.37982
315.15	0.6301	-6.95979	1210.493555	-3.86309

Table S26. Isentropic compressibility for LSNR, B@LSNR at variable temperatures.

T.(K)	Nd_2S_3 (10^{-7})	$Eu_2S_3(10^{-7})$	$Er_2S_3(10^{-7})$	$Yb_2S_3(10^{-7})$	$Nd_2S_3@Gd(10^{-7})$	$Eu_2S_3@Gd(10^{-7})$	$Er_2S_3@Gd(10^{-7})$	$Yb_2S_3@Gd(10^{-7})$
283.15	4.77	4.76	4.76	4.76	4.77	4.76	4.76	4.7
288.15	4.65	4.65	4.65	4.65	4.65	4.65	4.65	4.65
298.15	4.48	4.47	4.48	4.48	4.48	4.48	4.48	4.48
310.15	4.34	4.34	4.34	4.34	4.34	4.34	4.34	4.34
315.15	4.30	4.29	4.30	4.30	4.30	4.29	4.30	4.30

Table S27. Isentropic compressibility for B@LGT at variable temperatures.

Temp.(K)	$B: Nd_2S_3@GO(10^{-7})$	$B: Eu_2S_3@GO(10^{-7})$	$B: Er_2S_3@GO(10^{-7})$	$B: Yb_2S_3@GO(10^{-7})$
283.15	4.76	4.76	4.76	4.76
288.15	4.65	4.65	4.65	4.65
298.15	4.48	4.48	4.48	4.48
310.15	4.34	4.34	4.34	4.34
315.15	4.29	4.29	4.30	4.29

Table S28. Comparative study of lanthanide doping with metal sulphide/oxide with photocatalytic reduction of organic dyes.

Materials	Year	Doping route	Dopant	PCR	Study review	Ref.
(i) ZnS NPs		(i) Hydrothermal at 180 °C	(i) Pr	(i) Blue 19 reduced in 120 min	(i) Pr doped with ZnS for degrading reactive Blue 19 under visible light irradiation, highest decolorization with 3% Pr-doped ZnS NPs.	2
(ii) (Nd–TiO2) decorated on GO	2016	(ii) By sol–gel method at 60°C	(ii) Nd	(ii) Indigo carmine reduced in 3h	(ii) Nd doped with TiO_2 decorated on GO by sol–gel method. Nd–TiO_2–GO photocatalytic degraded indigo carmine under simulated solar light.	3
$FeMoO_4$	2017	Hydrothermal at 150°C	Eu^{3+} and Tb^{3+}	MB reduced in 60 min	Eu^{3+} and Tb^{3+} doped with $FeMoO_4$ nanorods and composites synthesized with GO and PCR a MB dye in visible light, enhanced photocatalytic efficiency than bare $FeMoO_4$.	4
(i) In_2S_3	2018	(i) Hydrothermal at 180°C	Yb^{3+}/Tm^{3+}	(i) Reduction of Cr^{6+} and Rh B in 100 min	(i) Yb^{3+}/Tm^{3+} co-doped with In_2S_3 synthesized for PCR of Cr(VI) and RhB. Doping with Yb^{3+}/Tm^{3+} did not change crystallinity of In_2S_3 but induced intermediate energy states for charge separation.	5
(ii) ZnS		(ii) Post-annealing process at 400°C	(ii) La	(ii) Turquoise Blue H5G reduced in 200 min	(ii) La doped with ZnS for photocatalytic degradation and ferromagnetic properties. Long-range ferromagnetism in La-ZnS nanostructures with vacancies and lattice deformation.	6
(iii) Fe-Gd-P tri-doped TiO_2 nanoparticles		(iii) Modified sol-gel method at 450°C	(iii) Gd	(iii) MO and 4-chlorophenol (4-CP) reduced in 180 min	(iii) Fe-Gd-P tri-doped TiO_2 NPs synthesized by modified sol-gel method, photodegraded MO and 4-chlorophenol (4-CP) in visible light. Gd increased oxygen vacancies and organic species on TiO_2 surface transferring photo-induced charge carriers to surface adsorbed species.	7

(i) TiO_2 (ii) TiO_2 nanoparticles (iii) TiO_2 (iv) La-ZnO, Ho-ZnO and Ce-ZnO NPs	2019	(i) Hydrothermal at 600°C (ii) Sol-gel method at 450°C (iii) Solvothermal at 900°C (iv) Sonochemical method at 300°C	(i) La and GO (ii) Ce, Dy, Lu, and Sm (iii) La^{3+} and Yb^{3+} (iv) La, Ho, Ce	(i) MB reduced in 40 min (ii) Caffeine reduced in 120 min (iii) Phenol reduced in 270 min (iv) Reactive Orange (29) reduced in 250 min	(i) PCR activities of TiO_2 incorporating La and GO, La modified recombination rate of photogenerated electron-hole charges on TiO_2. (ii) PCR degraded caffeine under visible light, high photoactivity with Ln to generate ions scavenged caffeine. in visible light. (iii) La^{3+} and Yb^{3+} doped TiO_2 reducing GO by solvothermal extending photocatalysis wastewater with high salt concentration. (iv) La-ZnO, Ho-ZnO and Ce-ZnO photocatalyzed reactive orange 29 (RO29) solution via sono-photocatalysis under visible light irradiation.	[8] [9] [10] [11]
MoS_2	2020	Auto combusted at 600°C	La-doped yttria	No PCR	Tribological activity of nano lamellar GO, nucleophilic substitution by methionine yielding M-rGO and with lanthanum (7%)-doped yttria NPs as (La-Y_2O_3)-MoS_2. Tribological activity, ternary (La-Y_2O_3)-MoS_2-(M-rGO) synthesized.	[12]
Nd_2O_3/Mo(S,O)$_{3-x}$·0.34H_2O	2021	Calcination at 800°C	Nd	MO, Rh B, MB PCR in 120, 90, 90 min respectively.	Precipitation method at 95°C to synthesize visible light driven Nd_2O_3/Mo(S,O)$_{3-x}$·0.34H_2O. MO, Rh B, and MB did PCR in visible light.	[13]
(i) ZnS QDs (ii) $Sr_3Sn_2O_7$	2022	Hydrothermal method	(i) Gd (ii) La or Nd	(i) Acid red 14 (AR14) and bisphenol-A (BA) reduced 180 min (ii) Crystal violet reduced in 120 min	(i) Gd^{3+} in ZnS QDs lattice enhanced PCR of QDs. GO and graphitic carbon nitride (g-C_3N_4) assessed its photocatalytic activity degrading acid red 14 (AR14) and bisphenol-A in visible light. (ii) La or Nd doped with $Sr_3Sn_2O_7$ synthesized via facile hydrothermal route. Rare earth metal doped hexahydroxy strontium stannate of high stability reusable for crystal violet degradation.	[14] [15]
CdS	2022	Microwave irradiation	La, Sm, Nd, Ce, Gd	MB reduced in 90 min	La, Sm, Nd, Ce, Gd doped CdS grafted reduced GO nanocomposites estimated in visible light, tunable band gap and high surface to volume ratio PCR a MB dye.	[16]
Nd_2S_3, Eu_2S_3, Er_2S_3, and Yb_2S_3	Present study	Monodispersion method at NTP	Gd	BBR reduced in 30 min	Series of LSNRs (Nd_2S_3, Eu_2S_3, Er_2S_3, and Yb_2S_3) synthesized via crash reaction methodology at NTP doped with Gd^{3+} and coated with GO has elaborated role 4f electron on shortening bandgap energies. PCPs predicted a least amount of photocatalysts to reduce 40 ppm BBR dye in 30 min with maximum reusability.	--

Table S29. ICP-0ES analysis for LSNRs, B@LSNRs, and B@LGTs.

Mean data ID: Nd_2S_3				Seq. No.: 1	Date: 27-12-2024 14:24:30	
Sample Qty: Analyte	Corresponding Intensity(g)	Prep. Vol.: Conc. (Calib)	Dilution: Std. Dev. Calib Units	Conc. (Sample)	Sample units	RSD
Nd 406.109	1334.4	4.513	mg/L	4.513	mg/L	%
Eu 381.967	11584.6	-1.094	mg/L	-1.094	mg/L	%
Er 337.271	-16620.4	-1.202	mg/L	-1.202	mg/L	%
Yb 328.937	513.3	-0.538	mg/L	-0.538	mg/L	%
Gd 342.247	827.0	-1.091	mg/L	-1.091	mg/L	%

Mean data ID: Eu_2S_3				Seq. No.: 2	Date: 27-12-2024 14:26:02	
Sample Qty: Analyte	Corresponding Intensity(g)	Prep. Vol.: Conc. (Calib)	Dilution: Std. Dev. Calib Units	Conc. (Sample)	Sample units	RSD
Nd 406.109	3358.5	-1.268	mg/L	-1.268	mg/L	%
Eu 381.967	1694409.6	4.429	mg/L	4.429	mg/L	%
Er 337.271	-16535.9	-1.201	mg/L	-1.201	mg/L	%
Yb 328.937	519.5	-0.557	mg/L	-0.557	mg/L	%
Gd 342.247	671.1	-1.097	mg/L	-1.097	mg/L	%

Mean data ID: Er_2S_3				Seq. No.: 3	Date: 27-12-2024 14:27:39	
Sample Qty: Analyte	Corresponding Intensity(g)	Prep. Vol.: Conc. (Calib)	Dilution: Std. Dev. Calib Units	Conc. (Sample)	Sample units	RSD
Nd 406.109	-53.6	-0.742	mg/L	-0.742	mg/L	%
Eu 381.967	2353.7	-1.118	mg/L	-1.118	mg/L	%
Er 337.271	74385.78	4.223	mg/L	4.223	mg/L	%
Yb 328.937	145.3	-0.582	mg/L	-0.582	mg/L	%
Gd 342.247	-635.6	-1.145	mg/L	-1.145	mg/L	%

Mean data ID: Yb_2S_3				Seq. No.: 4	Date: 27-12-2024 14:39:08	
Sample Qty: Analyte	Corresponding Intensity(g)	Prep. Vol.: Conc. (Calib)	Dilution: Std. Dev. Calib Units	Conc. (Sample)	Sample units	RSD
Nd 406.109	209.1	-0.588	mg/L	-0.588	mg/L	%
Eu 381.967	15539.7	-1.084	mg/L	-1.084	mg/L	%
Er 337.271	-17375.4	-1.216	mg/L	-1.216	mg/L	%
Yb 328.937	1543.1	4.783	mg/L	4.783	mg/L	%
Gd 342.247	429.9	-1.106	mg/L	-1.106	mg/L	%

Mean data ID: B@Nd_2S_3				Seq. No.: 5	Date: 27-12-2024 14:41:14	
Sample Qty: Analyte	Corresponding Intensity(g)	Prep. Vol.: Conc. (Calib)	Dilution: Std. Dev. Calib Units	Conc. (Sample)	Sample units	RSD
Nd 406.109	3806	4.150	mg/L	4.150	mg/L	%
Eu 381.967	12937.3	-1.091	mg/L	-1.091	mg/L	%
Er 337.271	-17755.4	-1.224	mg/L	-1.224	mg/L	%
Yb 328.937	1444.0	-1.171	mg/L	-1.171	mg/L	%
Gd 342.247	9831.9	1.763	mg/L	1.763	mg/L	%

Mean data ID: B@Eu_2S_3				Seq. No.: 6	Date: 27-12-2024 14:42:41	
Sample Qty: Analyte	Corresponding Intensity(g)	Prep. Vol.: Conc. (Calib)	Dilution: Std. Dev. Calib Units	Conc. (Sample)	Sample units	RSD
Nd 406.109	1648.2	-0.260	mg/L	-0.260	mg/L	%
Eu 381.967	1623457.4	3.974	mg/L	3.974	mg/L	%
Er 337.271	-17944.3	-1.227	mg/L	-1.227	mg/L	%
Yb 328.937	126.2	-0.640	mg/L	-0.640	mg/L	%
Gd 342.247	21394.0	1.341	mg/L	1.341	mg/L	%

Mean data ID: B@Er_2S_3				Seq. No.: 7	Date: 27-12-2024 14:44:19	
Sample Qty: Analyte	Corresponding Intensity(g)	Prep. Vol.: Conc. (Calib)	Dilution: Std. Dev. Calib Units	Conc. (Sample)	Sample units	RSD
Nd 406.109	-6821.9	-1.730	mg/L	-1.730	mg/L	%
Eu 381.967	56684.7	-0.981	mg/L	-0.981	mg/L	%
Er 337.271	17697.5	3.822	mg/L	3.822	mg/L	%
Yb 328.937	737.7	-1.221	mg/L	-1.221	mg/L	%
Gd 342.247	36522.8	1.212	mg/L	1.212	mg/L	%

Mean data ID: B@Yb_2S_3				Seq. No.: 8	Date: 27-12-2024 14:45:56	
Sample Qty: Analyte	Corresponding Intensity(g)	Prep. Vol.: Conc. (Calib)	Dilution: Std. Dev. Calib Units	Conc. (Sample)	Sample units	RSD
Nd 406.109	321.3	-0.522	mg/L	-0.522	mg/L	%
Eu 381.967	11486.0	-1.095	mg/L	-1.095	mg/L	%
Er 337.271	-18017.8	-1.228	mg/L	-1.228	mg/L	%
Yb 328.937	44130.3	3.066	mg/L	3.066	mg/L	%
Gd 342.247	1527.9	1.162	mg/L	1.162	mg/L	%

Mean data ID: B:Nd_2S_3@GO				Seq. No.: 9	Date: 27-12-2024 14:47:40	
Sample Qty: Analyte	Corresponding Intensity(g)	Prep. Vol.: Conc. (Calib)	Dilution: Std. Dev. Calib Units	Conc. (Sample)	Sample units	RSD
Nd 406.109	101043.6	2.326	mg/L	2.326	mg/L	%
Eu 381.967	8483.3	-1.102	mg/L	-1.102	mg/L	%
Er 337.271	-17185.3	-1.213	mg/L	-1.213	mg/L	%
Yb 328.937	391.6	-0.168	mg/L	-0.168	mg/L	%
Gd 342.247	212602.0	1.639	mg/L	1.639	mg/L	%

Mean data ID: B:Eu_2S_3@GO				Seq. No.: 10	Date: 27-12-2024 14:49:16	
Sample Qty: Analyte	Corresponding Intensity(g)	Prep. Vol.: Conc. (Calib)	Dilution: Std. Dev. Calib Units	Conc. (Sample)	Sample units	RSD
Nd 406.109	158.2	-0.618	mg/L	-0.618	mg/L	%
Eu 381.967	644080.9	2.502	mg/L	2.502	mg/L	%
Er 337.271	-17806.8	-1.225	mg/L	-1.225	mg/L	%
Yb 328.937	186.7	-0.456	mg/L	-0.456	mg/L	%
Gd 342.247	10172.0	1.750	mg/L	1.750	mg/L	%

Mean data ID: B:Er_2S_3@GO				Seq. No.: 11	Date: 27-12-2024 14:50:47	
Sample Qty: Analyte	Corresponding Intensity(g)	Prep. Vol.: Conc. (Calib)	Dilution: Std. Dev. Calib Units	Conc. (Sample)	Sample units	RSD
Nd 406.109	-1400.6	-1.536	mg/L	-1.536	mg/L	%
Eu 381.967	69048.9	-0.949	mg/L	-0.949	mg/L	%
Er 337.271	73521.4	2.451	mg/L	2.451	mg/L	%
Yb 328.937	15390.4	-1.081	mg/L	-1.081	mg/L	%
Gd 342.247	8703.4	1.439	mg/L	1.439	mg/L	%

Mean data ID: B:Yb_2S_3@GO				Seq. No.: 12	Date: 27-12-2024 14:52:17	
Sample Qty: Analyte	Corresponding Intensity(g)	Prep. Vol.: Conc.(Calib)	Dilution: Std. Dev. Calib Units	Conc. (Sample)	Sample units	RSD
Nd 406.109	-125.4	-0.785	mg/L	-0.785	mg/L	%
Eu 381.967	9689.7	-1.099	mg/L	-1.099	mg/L	%
Er 337.271	-5761.3	-0.999	mg/L	-0.999	mg/L	%
Yb 328.937	2027.4	2.216	mg/L	2.216	mg/L	%
Gd 342.247	290.3	1.111	mg/L	1.111	mg/L	%

References:

1 R. Saravanan, V. K. Gupta, V. Narayanan and A. Stephen, *J. Mol. Liq.*, 2013, **181**, 133–141.

2 Y. Hanifehpour, B. Soltani, A. R. Amani-Ghadim, B. Hedayati, B. Khomami and S. W. Joo, *J. Ind. Eng. Chem.*, 2016, **34**, 41–50.

3 S. O. B. Oppong, W. W. Anku, S. K. Shukla, E. S. Agorku and P. P. Govender, *J. Sol-Gel Sci. Technol.*, 2016, **80**, 38–49.

4 R. Singh, M. Kumar, H. Khajuria, S. Sharma and H. N. Sheikh, *Solid State Sci.*, 2018, **76**, 38–47.

5 Z. Wu, X. Yuan, G. Zeng, L. Jiang, H. Zhong, Y. Xie, H. Wang, X. Chen and H. Wang, *Appl. Catal. B Environ.*, 2018, **225**, 8–21.

6 N. Suganthi and K. Pushpanathan, *J. Mater. Sci. Mater. Electron.*, 2018, **29**, 13970–13983.

7 S. M. Adyani and M. Ghorbani, *J. Rare Earths*, 2018, **36**, 72–85.

8 L. L. Coelho, D. Hotza, A. S. Estrella, S. M. de Amorim, G. Li Puma and R. de F. P. M. Moreira, *J. Photochem. Photobiol. A Chem.*, 2019, **372**, 1–10.

9 V. O. Ndabankulu, S. Maddila and S. B. Jonnalagadda, *Can. J. Chem.*, 2019, **97**, 672–681.

10 T. Wang, B. R. Li, L. G. Wu, Y. B. Yin, B. Q. Jiang and J. Q. Lou, *Adv. Powder Technol.*, 2019, **30**, 1920–1931.

11 M. Sheydaei, M. Fattahi, L. Ghalamchi and V. Vatanpour, *Ultrason. Sonochem.*, 2019, **56**, 361–371.

12 N. Shukla, D. K. Verma, A. K. Singh, B. Kumar, Kavita and R. B. Rastogi, *ACS Appl. Nano Mater.*, 2020, **3**, 8012–8026.

13 S. Fentie Tadesse, D. H. Kuo, W. Lakew Kebede and G. Sisay Wolde, *Appl. Surf. Sci.*, 2021, **569**, 151091.

14 A. R. Amani-Ghadim, S. Arefi-Oskoui, R. Mahmoudi, A. T. Sareshkeh, A. Khataee, F. Khodam and M. S. Seyed Dorraji, *Chemosphere*, 2022, **295**, 133917.

15 A. Deng, C. Yu, Z. Xue, J. Huang, H. Pan and L. Pei, *J. Mater. Res. Technol.*, 2022, **19**, 1073–1089.

16 P. Devendran, D. Selvakumar, G. Ramadoss, R. Sivaramakrishnan, T. Alagesan, R. Jayavel and K. Pandian, *Chemosphere*, 2022, **287**, 132091.